Vacuum 190 (2021) 110282

Contents lists available at ScienceDirect

Vacuum

journal homepage: www.elsevier.com/locate/vacuum

Positron annihilation studies of irradiation induced defects in nanostructured titanium

K. Siemek [a,b,*], P. Horodek [a], V.A. Skuratov [b,c,d], J. Waliszewski [b,e], A. Sohatsky [b]

[a] Institute of Nuclear Physics Polish Academy of Sciences, PL-31342, Krakow, Poland
[b] Joint Institute for Nuclear Research, 141980, Dubna, Russian Federation
[c] National Research Nuclear University MEPhI, Kashirskoye sh. 31, 115409, Moscow, Russian Federation
[d] Dubna State University, Universitetskaya 19, 141980, Dubna, Moscow region, Russian Federation
[e] Faculty of Physics, University of Bialystok, K. Ciolkowskiego 1L, Bialystok, 15-245, Poland

ARTICLE INFO

Keywords:
Positron annihilation spectroscopy
Defects
Surface enhanced irradiation resistivity
Heavy ions
Grain size refinement
Surface mechanical treatment
Nanostructuration
Irradiation self-healing

ABSTRACT

The effect of irradiation doses and the role of grain size for titanium subjected to swift heavy 167 MeV Xe^{26+} ion irradiation have been investigated. Positron annihilation spectroscopy was applied for these studies. The nanostructured surface was obtained by blasting and annealing treatment. It was noticed that the concentration of vacancy clusters in the ion projectile range significantly decreased by a factor two after the grain size reduction. These clusters were built from 5 to 16 vacancies and were present mostly near the area occupied by the implanted atoms. Promising Ti properties as self-healing metal have been found. This study shows that grains structure strongly affects the resistivity of metals for irradiation and proves that surface mechanical treatments can be used as a grain size refinement method and modification of surface for enhanced irradiation resistivity.

1. Introduction

It is well known that many atomic defects occur in a target when it is irradiated. Defects can coalesce to form, for example, clusters of vacancies and dislocation loops. This leads to unwanted processes such as hardening, swelling, brittleness and creep, and ultimately to destruction of the material. It has been proven that the grain boundaries in the irradiated polycrystalline material can influence defects concentrations because they act as sinks where created defects disappear [1–8]. Therefore, grain size refinement was proposed as a solution for enhanced resistivity of nuclear materials under extreme irradiation conditions. In other words, the usability of such materials is extended without affecting their mechanical properties (i.e. strength and ductility). Better damage accumulation and lower defects concentration were observed in many nano- and ultrafine grain metals and their alloys, i.e. Ni [1], Cu [1], Mo [2], W [3], ferritic steel [4], austenitic steel [5], oxide dispersion strengthened steel [6], TiNi alloy [7]. For example authors [3] studied bubbles formation in W after 2 keV He ion implantation at 950 °C with two different ion fluencies of 3.6×10^{19} and 3.2×10^{20} ions/m^2 and they observed the presence of the grain size threshold equal 35 nm below which average bubble density drastically decreases. However, also in some studies lowering of mechanical properties due to an increase in grain size was noted, i.e. in nanocrystalline Cu irradiated with neutrons [8]. All this indicates the existence of an optimal grain size which should be assessed experimentally. The damage resistance issue in nanostructured metals is also important due to the possibility of applicability of such structures in electronics and space technology [9].

One of the promising approaches to prevent nuclear material degradation is the conception of self-healing material [10–14]. In such material irradiation damages under typical reactor operating conditions recover themselves. The self-healing properties depend strongly on the amount of grain and twins boundaries. A self-recovery mechanism was firstly described by atomic simulations for pure Cu [10]. Bai et al. [10] have shown that in nano-Cu upon irradiation, interstitials are loaded into the boundary, which then acts as a source, emitting interstitials to annihilate vacancies in the bulk. A similar mechanism was then proposed also for Fe [11]. In metals, self-healing remains challenging due to low atomic mobility at non-elevated temperatures [12]. However, the defect migration kinetics allow resolving this problem [13,14]. Only a few experiments confirm the self-healing idea in metals. Twin boundaries self-healing was observed by in situ studies in the heavy ion irradiated Ag and Cu [13,14]. Atomistic simulations reveal that nano-twins are essential to achieve superior radiation tolerance as twin boundary

* Corresponding author. Institute of Nuclear Physics Polish Academy of Sciences, PL-31342, Krakow, Poland.
E-mail address: siemek@jinr.ru (K. Siemek).

https://doi.org/10.1016/j.vacuum.2021.110282
Received 6 November 2020; Received in revised form 24 April 2021; Accepted 27 April 2021
Available online 1 May 2021
0042-207X/

networks promote rapid migration of defect clusters to nanovoids. Twins during radiation provide a continuous source for mobile interstitial loops which then can annihilate in nanovoids [14]. Reducing the grain sizes of coarse-grained face center cubic metal mostly reduces the propensity for deformation twinning [15]. The hexagonal close-packed structure is the most likely to form twinning deformation. The high-density twins were reported in nano- and ultrafine grain Ti [16]. Moreover, molecular dynamic simulations have shown that the elliptical self-interstitial cluster is a precursor in an irradiation-induced nano-twinning in Zr and Ti [17].

Nuclear materials have to withstand neutron irradiation for many years. The irradiation damages created by long time neutron exposition can be replaced by irradiation with heavy ions [18]. The implantation range of such ions is limited to several μm depths. The typical nanostructured area obtained by mechanical surface treatment significantly exceeds the range of the heavy ions. It means that fundamental microstructures changes caused by neutron degradation can be performed in a thin nanostructured surface prepared by easily applicable mechanical methods and heavy ions irradiation. Mechanical surface treatments allow one to get grain size in the surface region in wide ranges up to sizes even not available for typical methods exploiting high-pressure, like high pressure torsion, hydrostatic extrusion, equal channel angular pressing, etc. For example, the mean grain size of Ti (purity 99+%) acquired by surface mechanical attrition treatment was reported as 13.21 nm [19], when typically high-pressure methods can reach the size not lower than 50 nm [20–22]. This gives the possibility to study an irradiation degradation of nanostructured metals and also the application of surface treatments as a finishing method for enhanced surface radiation resistance.

The aim of the current studies is focused on studies of grain size role on irradiation resistance and evaluation of the self-healing Ti properties. According to knowledge of the authors, irradiation damages in Ti have not been studied exhaustingly and only few reports associated with irradiation resistance of Ti or its alloys can be found [23–26]. For example, Budzynski et al. [23] have shown that after implantation of heavy 130 MeV Xe ions the new hcp structure is formed whose lattice parameters are about 10% larger than those of the original material. In this work authors also noted 13% increase of hardness for fluence 10^{14} ions/cm^2 caused by presence of the defects. Previously, positron annihilation studies for coarse grain Ti sample [24] shown that dislocations and vacancies clusters are observed in projectile ion range and no additional damages induced by irradiation stress appear over it. In the current work, we investigated the blasting and annealing technique as the example of a grain refinement method, which shows that nanostructuration of Ti can lead to solving the issue related to its microstructure degradation.

2. Experiment

Ti samples in shapes of plates 10 mm × 10 mm × 5 mm with purity 99.99% were annealed in 1000 °C for 4 h at vacuum 10^{-5} Pa. Residual gas atmosphere during annealing could be responsible for negligible contamination of samples surface but do not affect performed experiment. Titanium was chosen as a promising nuclear base material with a low neutron activation. It was shown that blasting and further low-temperature annealing of the aluminum and titanium surface can lead to forming well-ordered ultrafine or nanograin surfaces [27,28]. After annealing, samples were of the same condition, a glass-bead-blasting was performed to obtain a high density of dislocations. Blasting was made using 125 μm glass beads in a period of 5 min and overpressure 0.5 MPa bar at Renfert Vario Basic Jet. The blasting nozzle was directed perpendicularly to the surface at a distance of 10 mm. Then the blasted samples were annealed in 200 °C for 1 h. After that subsurface layer of 5 μm was removed by etching, which eliminates microcracks and retained glass. Two samples were kept as references and the other irradiated using heavy 167 MeV Xe^{26+} ions at Flerov Laboratory of Nuclear Reactions at JINR, Russia. Four different fluencies were used 5 × 10^{12}, 10^{13}, 5 × 10^{13}, 10^{14} ions/cm^2. The average ion flux was 5 × 10^9 ions/(s × cm^2). One additional annealed coarse grain sample intended for TEM examination was irradiated with dose 10^{12} ions/cm^2.

3. Methods

Doppler broadening of annihilation line and Positron Annihilation Lifetime Spectroscopy (PALS) are two most promising and unique methods allowing one to get knowledge about the type and irradiation defect concentration in a very shallow depth, especially when they employ Variable Energy Positron (VEP) beam. They application in different problems was proven many times [29–35].

VEP measurements were performed at JINR in Dubna, Russia [36]. The energy of incident positrons, which are implanted into a sample ranged from 50 eV to 34 keV. It corresponds to the implantation depth up to 2.3 μm in titanium. In this measurement only the Doppler broadening of annihilation line was monitored. For this purpose HPGe detector ORTEC GEM25P4-70 with an energy resolution (FWHM) of 1.20 keV at 511 keV was used. The annihilation line shape parameter S was evaluated in a function of incident positron energies of the beam. It is defined as a ratio of the area below the center of the annihilation line to the total area of the peak. The S parameter value reflects the fraction of positron annihilation with low momentum electrons mainly present in defects. Two parts of the same samples were studied after irradiation: the so-called track region, and the cascade region. The track region is defined as a zone in which ion loses its energy mostly interacting with electrons. This region precedes the highly damaged region in which the atomic collision cascade occurs.

The conventional PALS measurements were performed using digital spectrometer APU-8702RU with detectors based on the BaF_2 scintillators. The timing resolution (FWHM) equaled about 180 ps. The positron source was based on ^{22}Na with activity 27 μCi closed between thin 5 μm thick titanium foils and its contribution was equal to 14%. Source contribution consists of two lifetime components: 242 ps (97%) and 952 ps (3%) and was subtracted during spectra deconvolution. The analysis of obtained spectra including 2 × 10^6 counts was provided with the LT program [37]. The average penetration depth of ^{22}Na positrons into Ti is about 48 μm [38]. To get information on defects depth distributions a sequential etching procedure was applied. Each sample was etched in a solution of 10 ml HNO_3, 2 ml HF and 10 ml distilled water to reduce their thickness and then a positron lifetime spectrum was measured. This procedure was repeated until the bulk value of a positron lifetime was obtained. The etching does not cause the formation of additional defects and this procedure was successfully used in many studies [24,29,30].

The XRD measurements have been performed at room temperature using the Roentgen diffractometer EMPYREAN in Frank Laboratory of Neutron Physics, Dubna, Russia. A water-cooled X-Ray tube with Co anode was used as a source of radiation. The data acquisition system is based on a silicon strip detector PIXcel 1D that contains 255 strips and covers a range of (0°–3.5°) in 2θ angular scale. The depth of analysis is equal to around 13 μm (measured in the direction normal to the sample surface).

The TEM study was carried out using TalosF200i transmission electron microscope operating at an accelerating voltage of 200 kV.

4. Results and discussion

4.1. PALS results for samples after blasting and refinement process

Shot damage causes typical defects of plastic deformation in the surface area, and therefore there are dislocations and vacancies in the crystal structure. First, we examined the depth distribution of defects in the sample after shot blasting and in the sample further annealed at 200 °C for 1 h (called later also as refinement sample). It should be noted

that the used temperature of 200 °C, for the creation of ultrafine well-ordered grains, is comparable with the planned operating temperature of high strength titanium alloys in International Thermonuclear Experimental Reactor (ITER) components, and is a little lower than the temperature in II generation fission reactor vessel [25,39]. In Fig. 1 the positron lifetimes of the samples before and after annealing of the blasted surface are depicted. For well annealed initial samples positron lifetime was equal to 147 ps, and corresponded with Ti value for not defected bulk structure [40,41], (hatched area in Fig. 1 a, e). The mean positron lifetime is defined as:

$$\overline{\tau} = \sum_i \tau_i \times I_i, \tag{1}$$

where τ_i, I_i are positron lifetime components and corresponding intensities, resolved from the measured PALS spectrum. Each lifetime component stands for different defect types and its intensity correlates with its concentration. After treatments mean positron lifetime $\overline{\tau}$ below the surface increases, see Fig. 1a, e. The damaged region with defects spreads up to 100 μm for blasted - Fig. 1a, and 150 μm for refinement samples - Fig. 1e. Some parts of positron emitted from ^{22}Na isotope can reach undamaged part of sample and annihilate with positron lifetime equal 147 ps. Its number was determined using LYS-1 program based on multi scattering model described in detail in work [42]. During calculations an experimental geometry of measurements and Ti absorption coefficient equal 208 cm^{-1} was used. The amount of positrons which annihilate in undamaged material increase nonlinearly with cumulative thickness of removed material, see Fig. 1d and h. During deconvolution of spectra one lifetime component τ_3, standing for positrons annihilated in undamaged part, was fixed. In the blasted sample we recognize two additional positron lifetime components standing for different types of defects in damaged part of sample. The first one with intensity over 80% with a lifetime of 170–180 ps stands for dislocations. Similar lifetimes 178 ps (I = 78%) were reported in ultrafine-grained Ti–6Al–4V titanium alloy with a grain size around 290 nm [31] and also in severe plastic deformed Ti, where τ = 185ps (I = 98.4%) [32]. Longer lifetime component with values from 310 to 340 ps represents small vacancy clusters. Their size can be estimated as 4–6 vacancies based on calculations performed for pure Ti at work [32]. These observations agree with calculations of V_1–V_3 vacancy cluster energy formation, which shows that bigger vacancy clusters, like trivacancies is much more stable than mono- and divacancy [33]. In the damaged region, the values of τ_1 and τ_2 remain almost constant up to 40 μm. After refinement (annealing), the long component almost disappears. Only near-surface (refinement sample without etching) the presence of τ_4 component 1120 ps was observed which is caused by clustering vacancies and microcracks. Authors [28] studied surface roughness of blasted and refinement Ti sample. Similarly, the presence of 5 μm depth cracks was observed only in the annealed samples. In the refinement sample spectra, three components were found. The first one τ_1 with lifetimes around 170 ps represents dislocations that formed grain boundaries during Ti recovery (Fig. 1f) and the second one is a reduced bulk lifetime inside grains in damaged part of sample, which responds to a delocalized positron

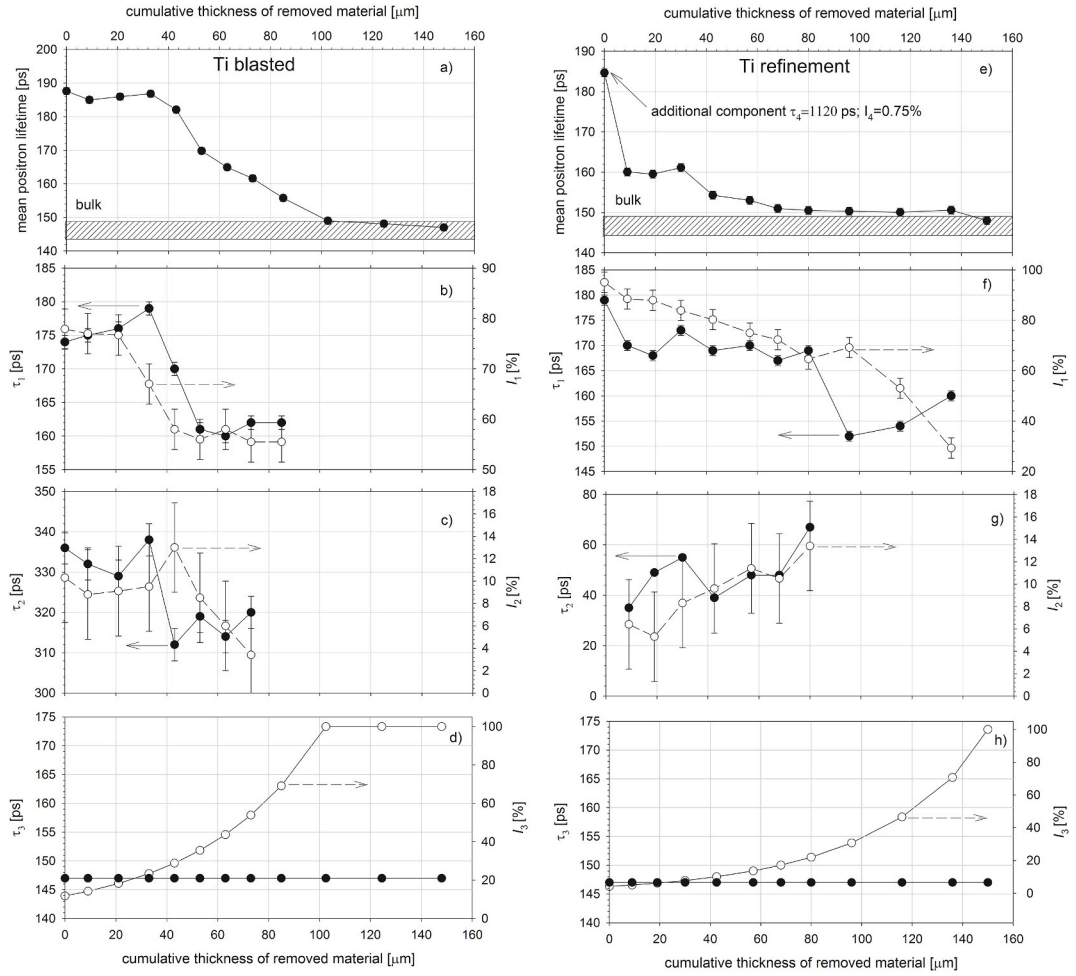

Fig. 1. The depth profile of the fitted positron lifetime components τ_1, τ_2, fixed component τ_3 and the mean positron lifetime obtained for the sample exposed to blasting and after grain refinement (blasting and annealing). Open points represent components intensities. The hatched area marked the positron lifetime value measured on the sample before treatment.

annihilation from the Bloch-state (Fig. 1g). Similarly to blasted sample, the third component represents the positron annihilated in the undamaged region. Corresponding intensities I_1 and I_2, illustrating the number of positrons annihilating in a given type of defect, are marked as open points at the same plots. It should be mentioned that over 80 μm a deconvolution of spectra was done with only two positron lifetime components i.e. τ_1 and τ_3. Fitting using three components causes in this case a lack of physical interpretation of obtained results because a few-ps lifetimes τ_2 with very small intensities are generated. However, it is expected that τ_2 will rise at depths close to the undamaged region. In this way the separation of τ_2 from τ_3 over 80 μm cannot be performed. The presence of only one type of defect gives the possibility to evaluate grain size. For this purpose, we use the relationship that links the value of the average positron lifetime with the grain diameter d_0, in accordance with the model of the diffusion-reaction controlled trap [34,43]:

$$\overline{\tau} = \tau_f + 6\frac{L_+}{d_0}(\tau_b - \tau_f)\frac{L(d_0/2L_+)}{1+\frac{L_+}{\alpha}\frac{}{\tau_f}L(d_0/2L_+)}, \quad (2)$$

where α is positron specific trapping rate at a grain boundary, L_+ is the positron diffusion length inside the grain, τ_f is the positron lifetime in the grain, and d_0 is its diameter, $L(z) = \coth(z) - 1/z$, is the Langevin function. A typical for metals $L_+ = 180$ nm and $\alpha = \infty$ m/s (which means that all positrons are trapped by grain boundaries) were assumed in calculations. In Fig. 2, the above function equation (2) was plotted in dependency on grain size. Obtained results indicate that mean grain size averaged over the positron implantation profile in the region up to 40 μm remains in the diameter range from 470 to 540 nm. This grain size is bigger than the one in blasted under pressure 0.3 MPa and further annealed in 150 °C pure aluminum, where the mean grain size according to XRD and TEM studies was in the range 50–70 nm [27]. It is also bigger than the grain size equal to 50 nm (based on XRD studies) reported after refinement of the Ti surface blasted with SiO_2 particles driven by 2.07 MPa compressed air [28] and the value of 180 nm reported in the top of the ultrafine grain layer of Ti after mechanical shot blasting [44]. The obtained positron data was compared with grain size obtained by XRD method. In Fig. 3 the patterns for initial samples annealed at 1000 °C and samples after grain refinement are shown. The grain size for blasted and annealed samples was evaluated using Scherrer method [45] for reflection (001) and (002) and it was equal to 33 nm. The size of

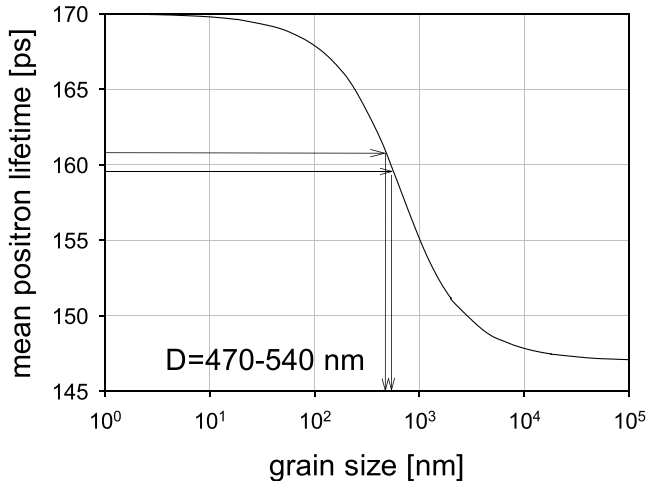

Fig. 2. Estimation of grain size D in ultrafine subsurface obtained after refinement method. The black line illustrates the mean positron lifetime calculated using equation (2) with parameters $\alpha = \infty$ ms^{-1}, $L_+ = 180$ nm, $\tau_F = 147$ ps, $\tau_B = 170$ ps. The horizontal arrow is the mean positron lifetimes measured for ultrafine surfaces and the vertical line shows estimated grain size.

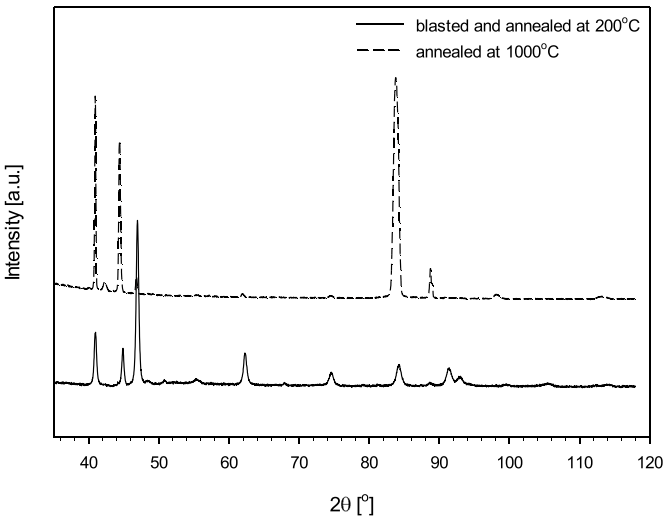

Fig. 3. The XRD pattern for the Ti sample annealed at 1000 °C for 4 h (dashed line), and for the sample blasted and annealed at 200 °C for 1 h (solid line).

hexagonal Ti unit cell obtained from XRD measurements decrease from value 35.58 Å^3 (lattice constants a = b = 2.9492(19) Å, c = 4.7234(25) Å) to 35.47 Å^3 (a = b = 2.9539(3) Å, c = 4.6935(8) Å) indicating presence of residual compressive stresses. It could be assumed that the grain size in the top of the surface is much smaller and changes sharply with increasing depth but it cannot be estimated exactly from the performed positron experiment due to the broad positron implantation profile (the average penetration depth is 48 μm). The few dozen μm thicknesses of the obtained ultrafine layers are similar to this reported in Al [27] and Ti [28] after blasting and is smaller than the size of the ultrafine grain Ti in work [44], which on dependency of used machine blasting parameters reach even 320 μm. All these show that the thickness of the ultrafine layer and its grain size can be controlled by different blasting parameters like particle size, blasting duration, and propelled force.

4.2. VEP results for samples after irradiation

In a refinement sample before irradiation, a 5 μm layer was etched. Such samples will be called UltRef (Ultrafine Reference). These samples were irradiated with Xe^{26+} swift ions. The impact of one heavy ion in the track region is comparable to more than 10^5 neutrons. The dose in dpa (displacements per atom) and Xe atom distributions below the Ti surface were obtained using SRIM/TRIM [46] calculation for 10^{14} Xe^{26+} ions/cm^2, and are presented in Fig. 4a.

The projectile range of the ions is about 13 μm. The maximum damages corresponding to the Bragg peak position are observed at 11.8 μm. For this reason, both ion track region and cascade area (the sample after additional etching of 11 μm) were investigated using a positron beam. The results of these measurements presented as S parameter in the function of implanted positron energies are shown in Fig. 4b and c. The upper axis corresponds to the mean implantation depth of positron evaluated according to the formula:

$$\overline{z} = \frac{A}{\rho}E^n, \quad (3)$$

where A and n are the Makhov function parameters and $\rho = 4.5$ g/cm^3 is the density of titanium. The values $n = 1.655$ and $A = 2.86$ μgcm^{2}keV^n reported for Ti were used in evaluation [47].

In the ion track region, the S parameter does not vary significantly for all samples, except the near surface region at the depth less than 50 nm, which can be caused by the surface roughness and oxides, Fig. 4b. In addition, the difference between irradiated and UltRef samples is almost

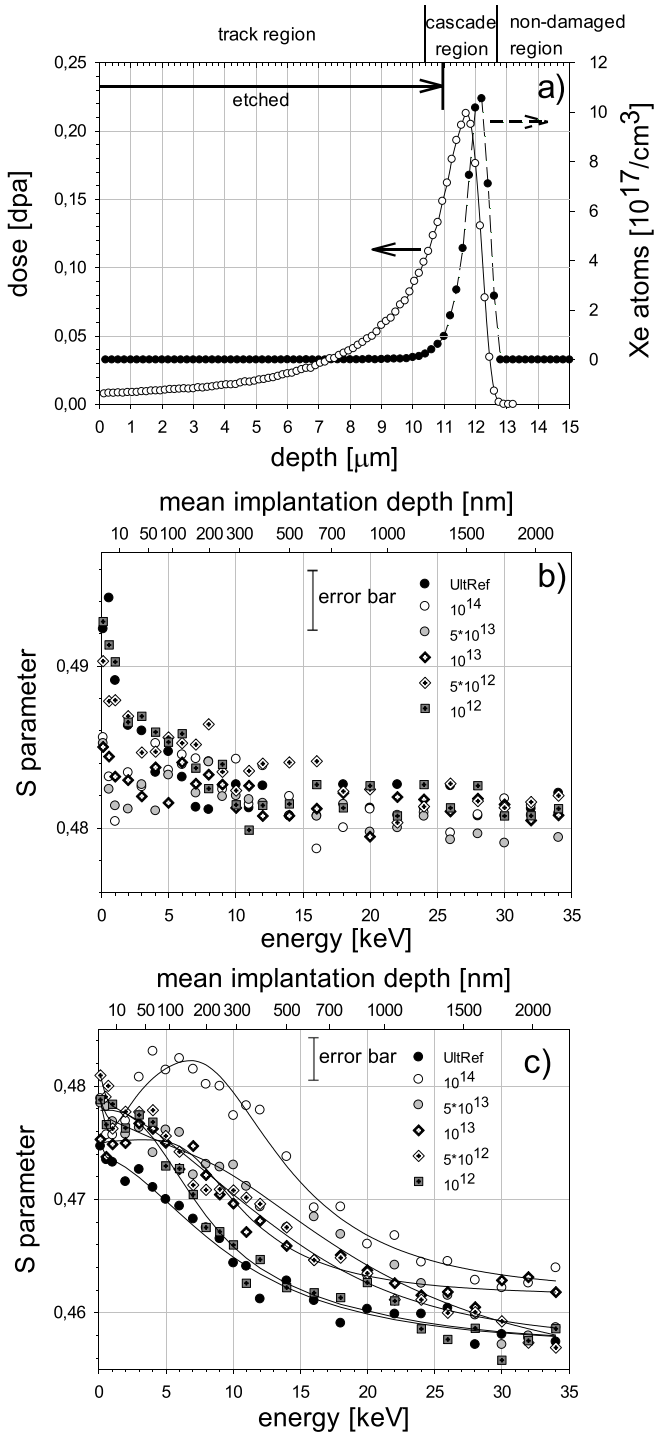

Fig. 4. SRIM/TRIM calculations of dose and implanted atoms distribution after 167 MeV Xe^{26+} ion irradiation to titanium with fluencies 10^{14} ion/cm^2 is shown in a). The determined S parameter in the function of positron energies performed using variable energy positron beam is presented in b) and c). The upper axis corresponds to the mean implantation depth obtained using equation (3). The results for the track area are shown in b) and for cascade region (after etching of 11 μm) in c). The solid lines present best fits obtained using VEPFIT software.

not observed indicating enhanced irradiation resistivity. Up to 2 μm, for the highest Xe^{26+} ion fluency the Ti metal gets a comparative dose equal ca. 0.01 dpa (see Fig. 4a). After etching a layer of 11 μm thick, the S parameter value of the UltRef sample in an interior decreases from value around 0.48 to 0.454, Fig. 4c. This can be explained as the result of the heterogeneity of the nanostructured layer and the growing grain size. The higher the irradiation dose, the greater the number of defects, which increases the value of the S parameter, see Fig. 4c. For the highest dose, even a maximum at the depth of 150 nm is visible. The obtained relationships can be described with the VEPFIT [48] program, which takes into account the diffusion of positrons near the entrance surface. A two-layer model was assumed. Each layer has its own value of diffusion length L_+, S parameter, and thickness. During fitting a positron diffusion length for second layer was fixed to 180 nm. The best fits are plotted as the solid lines in Fig. 4c. Corresponding to them parameters are shown in Fig. 5. It should be noted that the S parameter rises in the first layer from 0.461 up to 0.484, and L_+ decreases from 181 to 49 nm with increasing fluency indicating the increased number of structural defects in the cascade region. The fitted size of this region is around 500 nm, however, its accuracy is limited by the etching procedure. The sample thickness after etching was measured using a micrometer screw with uncertainty around ±500 nm. Therefore, it should be assumed that this region corresponds well with SRIM/TRIM calculations. Over this region only in the sample irradiated with dose 10^{13} and 10^{14} slightly increased value of the S parameter exists.

4.3. PALS results for samples after irradiation

The types of defects and its profile after irradiation for ultrafine grain sample was determined using PALS and compared with previous results performed for coarse-grain sample described in details in Ref. [24]. In Fig. 6 both results irradiated with dose 10^{14} ions/cm^2 are shown. Two lifetime components can be separated from spectra at each depth. In a coarse grained sample, see Fig. 6 c, a longer lifetime in the range from 320 to 400 ps can be described as clusters of 5–16 vacancies, however, this estimation does not take into account the presence of implanted Xe atoms. It is known that Xe atoms can create XeV_n vacancy complexes in metals [49]. Similar defects occur also for ultrafine grained samples, Fig. 6 f. Therefore, the size of clusters does not depend on the size of the grains, and the influence of the irradiation dose was also not noted. Lack of mono- and divacancies indicates its mobility at room temperature. Indeed, the self-migration energy of these vacancies is below 0.60 eV and migration is easier for the divacancies than for the monovacancy [33,50]. It means that at room temperature stable V_3 is immobilized and initiates the formation of a larger cluster. Smaller vacancy clusters can join such clusters or annihilate at the grain and twin boundaries. The presence of vacancy clusters was confirmed in TEM measurements in coarse grain Ti sample irradiated with fluency 10^{12} ions/cm^2, see Fig. 7. Vacancy clusters occupy the depth up to 13 μm which corresponds well with the ion projectile range. In a coarse grain sample also the presence of dislocations up to 15 μm was found, indicated by τ_1 value larger than a bulk lifetime, see Fig. 6b. Over this region, no effect of irradiation was noted. For the ultrafine grain sample, over 13 μm depth, only grain boundaries (Fig. 6e) with lifetimes around 170 ps and delocalized positron annihilation inside grain can be found (see Fig. 6g). It is very similar to the blasted and annealed ultrafine sample in Fig. 1 d-f.

The most interesting changes occur in the intensity of the vacancy clusters component, which is linked with its concentration. In the case of a coarse grain sample, the intensity I_2 remains stable around 10% up to 5 μm, see Fig. 6 c, and it is twice as big as noted for the ultrafine grain sample - Fig. 6 f. The intensity of the second lifetime component I_2 for all doses as a function of depth is shown in Fig. 8 a-d for samples with the coarse grain (white points) and with ultrafine grain (black points). Also for other doses, the intensity of the vacancy cluster component is twice as high, while the positron lifetime values remain almost unchanged - Fig. 8 e-h. The concentration of these clusters should be then connected with the grain size. The intensity does not change significantly up to a depth of 7 μm. In this region the smallest number of vacancies was created (Fig. 4a), which due to the mobility of V_1–V_2 clusters mostly migrate to grain boundaries and annihilate before the creation of an

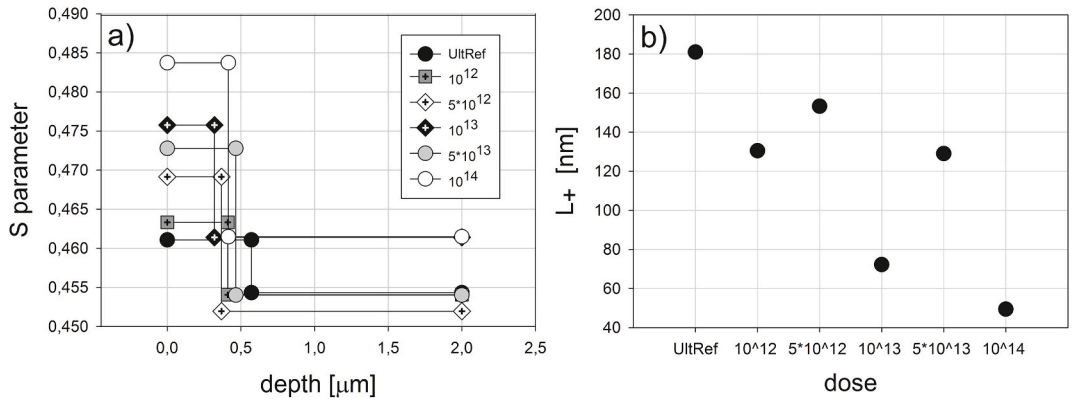

Fig. 5. S parameter depth distribution in the cascade region fitted using the VEPFIT program is shown in a). The positron diffusion length obtained for each sample is present in b). The best fits are shown as lines in Fig. 4c.

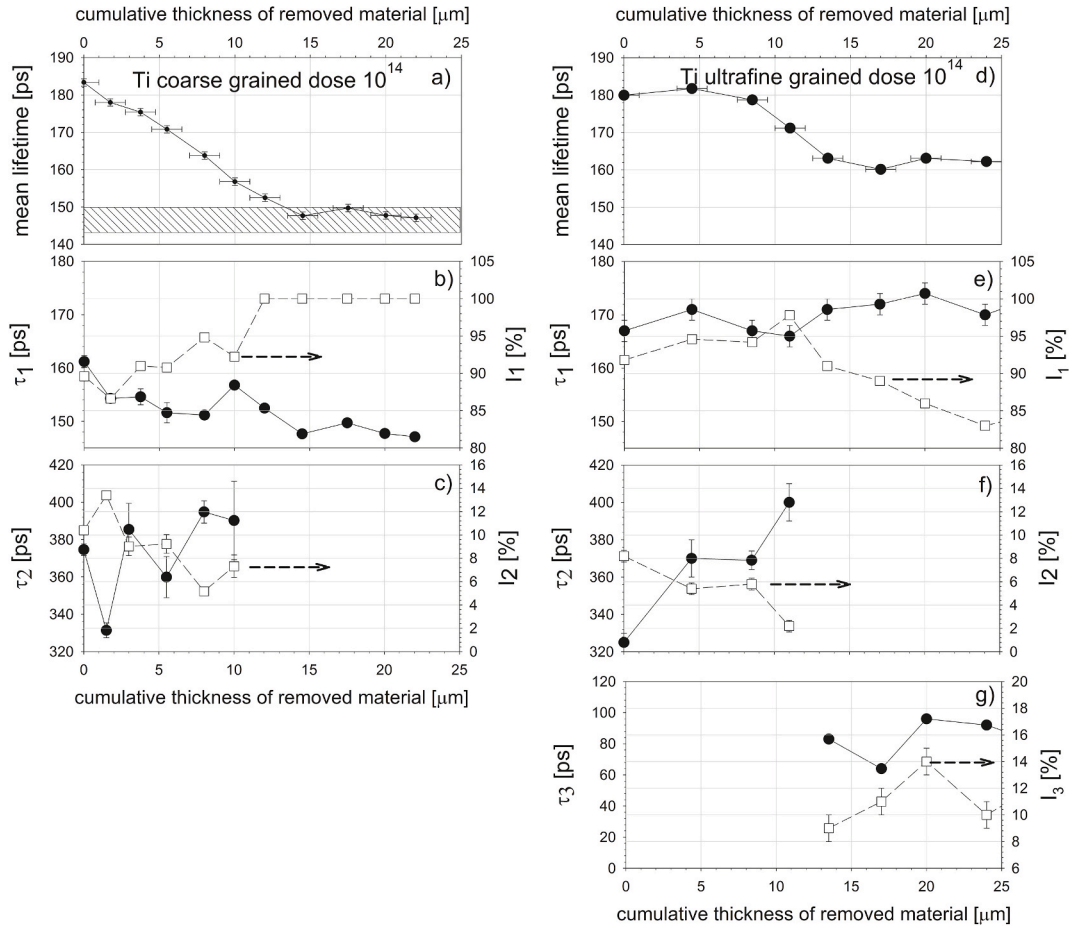

Fig. 6. Positron lifetime measurements results for Ti samples with coarse and ultrafine grain after irradiation with 167 MeV Xe^{26+} heavy ions with fluency 10^{14} ion/cm^2. In a) and d) the mean positron lifetime is presented. In b), c), e-g) positron lifetime components (black points) and their intensities (white points) in the function of the cumulative thickness of removed material are shown. They have been obtained after the deconvolution of spectra using the LT program [37]. The data for coarse grained sample was taken from work [24].

immobile bigger cluster. However, the intensity drops above 7 μm for coarse samples but not for samples with refinement grains. This informs us about the broader distributions of clusters in the coarse grain sample. The sink efficiency in the coarse grain sample is much smaller than for the ultrafine sample which results in increased formation of bigger clusters. In both cases all vacancy clusters are removed when cumulative etched depth reaches 13 μm and exceeds the range of ion implantation. This well agrees with the positron beam results for nanostructurated sample, where the S parameter is increased only in the Bragg peak position and does not change in track region. These vacancy clusters are located in the region in which implanted heavy atoms stay after irradiation (Fig. 4a). It can be expected that the presence of Xe atoms stabilizes and initiates the creation of these clusters. A similar effect was noted, i.e. in silicon doped with high doses of He [35]. A migration and accumulation of implemented atoms on grain boundaries results in bubble cluster formations, which are the origin of cracks [51]. However,

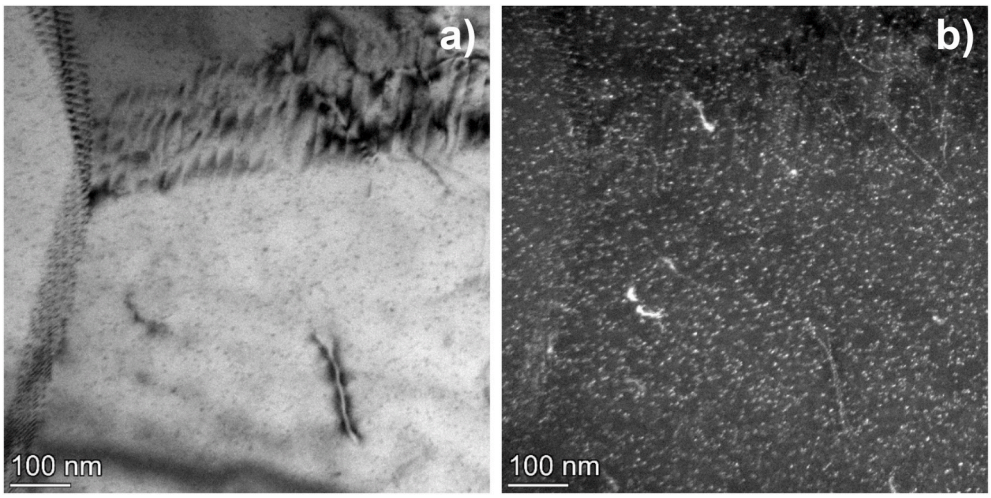

Fig. 7. TEM micrographs of Ti sample surface irradiated with swift heavy 167 MeV Xe^{26+} ions with fluency 10^{12} ions/cm^2. a) – Bright field image of a sample region with a triple junction of low-angle grain boundaries. b) – Dark field image of the same region in weak beam mode. Vacancy clusters are visible as small white spots in image b) or the same size dark spots in image a).

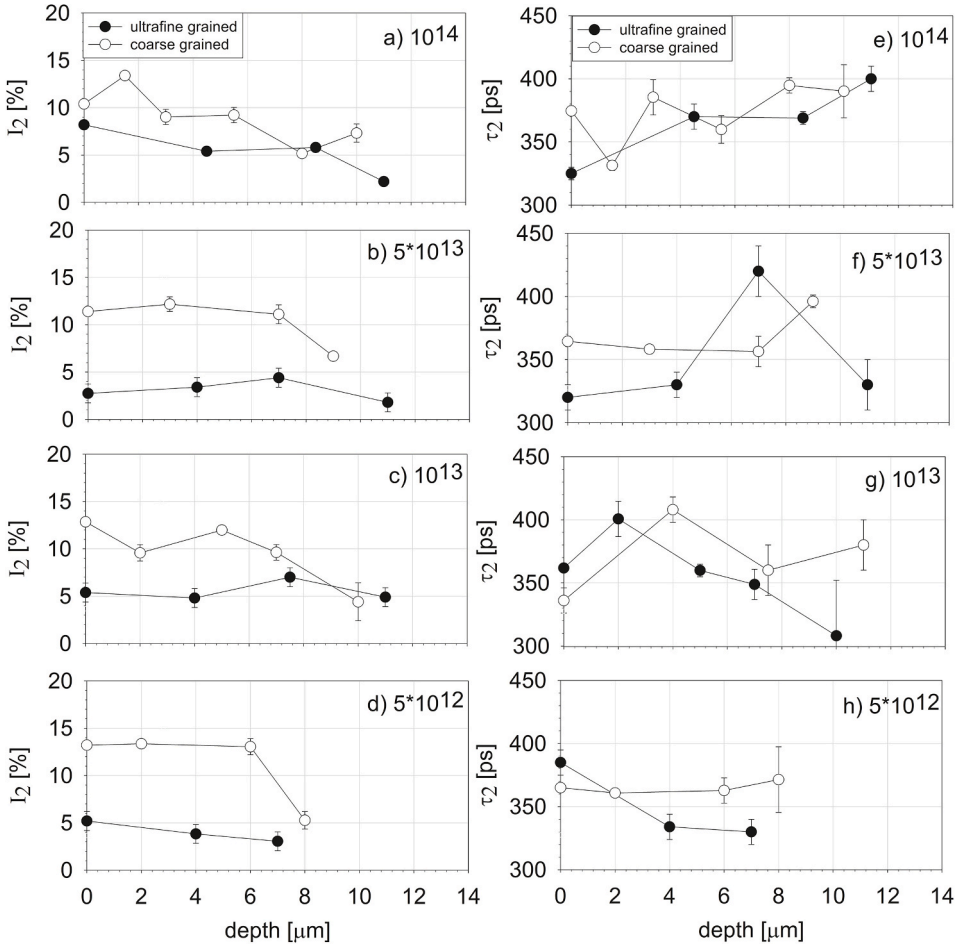

Fig. 8. The long component of positron lifetime τ_2 e-g) and its intensities I_2 a-d) for Ti samples with coarse (white points) and ultrafine grain (black points) after irradiation with 167 MeV Xe^{26+} heavy ions with fluencies 5×10^{12}, 10^{13}, 5×10^{13}, 10^{14} ion/cm^2.

due to large size of Xe atom its migration can be expected at higher temperatures. H.A. Vasco et al. [52] studied annealing of defects in TiN after Xe swift heavy ion irradiation and observed that the migration of Xe was by trapping and de-trapping in defects at temperatures below 1200 °C and was mainly through grain boundary diffusion at elevated temperatures. All this shows that decrease size of grains in Ti can limit the clusters concentration and reduce its occurrence to Bragg peak position.

It is known that Ti alloys are very sensitive to neutron irradiation, and even a relatively low dose of neutrons results in degradation of

ductility and fracture toughness [25]. This drastically limits Ti alloys in a nuclear application. Studies of neutron irradiated 64% cold worked by swaging Ti [26] have shown that the majority of cavities are found inside the grains of recrystallized Ti structure irradiated at 348 °C. The influence of material structure (smaller grain size and β′ precipitates) on its mechanical properties changes were observed in neutron irradiated high strength Ti–6Al–4V alloy [25]. The performed experiment has shown that problems with microstructure degradation can be solved by nanostructuration. The concentration of vacancy clusters can be lowered by grain refinement. If we provide fast migration channels like twins, in which small vacancy disappears before the creation of V_3 clusters, we will also observe efficient radiation damage recovery at room temperature. Moreover, according to the presented results, irradiation of pure nanostructured Ti in temperature 200 °C can lead to full recovery of structure. The disappearing of V_3–V_6 vacancy clusters produced during blasting was observed after annealing at 200 °C. In such temperature, these vacancies are mobile, or are unstable and dissociate down to V_1 and V_2 and then can easily migrate and be absorbed by sinks. This reveals that pure Ti and its alloys in equivalent nanoforms should be considered in places exposed also to high neutron doses up to recrystallization temperature of nano-Ti which is equal to around 400 °C [21, 22]. This temperature is enough for typical operation temperature in current II generation fission reactors. Nowadays, pure nano- and ultrafine grain Ti can be obtained using many currently available techniques based on high pressure [7–22] and it can possess better ductility and comparable or even higher strength than Ti–6Al–4V alloy [20].

5. Conclusion

Performed studies based on positron annihilation spectroscopy show that defects induced by irradiation are formed on the ion track. Most of them are present in the Bragg peak position and consist of 5–16 vacancies in clusters. The Xe^{26+} dose up to 10^{14} ions/cm^2 and grain size do not affect significantly the cluster size. However, its concentrations for the nanostructured sample are almost twice as small in comparison with coarse grain samples. VEP result indicates the lack of structural changes in the ion track region in nanostructured samples. The disappearing of vacancy clusters after annealing at 200 °C indicates promising self-healing property of Ti.

Declaration of competing interest

The authors declare that they have no known competing financial interests or personal relationships that could have appeared to influence the work reported in this paper.

Acknowledgment

The authors would like to thank J. Dryzek (from the Institute of Nuclear Physics Polish Academy of Sciences) for providing PALS experimental results of irradiated coarse grain samples and A.G. Kobets (from Joint Institute for Nuclear Research) for his technical support in VEP measurements.

References

[1] N. Nita, R. Schaeublin, M. Victoria, Impact of irradiation on the microstructure of nanocrystalline materials, J. Nucl. Mater. 329–333 (2004) 953–957, https://doi.org/10.1016/j.jnucmat.2004.04.058.
[2] G.M. Cheng, W.Z. Xu, Y.Q. Wang, A. Misra, Y.T. Zhu, Grain size effect on radiation tolerance of nanocrystalline Mo, Scripta Mater. 123 (2016) 90–94, https://doi.org/10.1016/j.scriptamat.2016.06.007.
[3] O. El-Atwani, J.A. Hinks, G. Greaves, J.P. Allain, S.A. Maloy, Grain size threshold for enhanced irradiation resistance in nanocrystalline and ultrafine tungsten, Mater. Res. Lett. 5 (2017) 343–349, https://doi.org/10.1080/21663831.2017.1292326.
[4] A. Alsabbagh, A. Sarkar, B. Miller, J. Burns, L. Squires, D. Porter, J.I. Cole, K. L. Murty, Microstructure and mechanical behavior of neutron irradiated ultrafine grained ferritic steel, Mater. Sci. Eng. A 615 (2014) 128–138, https://doi.org/10.1016/j.msea.2014.07.070.
[5] C. Sun, S. Zheng, C.C. Wei, Y. Wu, L. Shao, Y. Yang, K.T. Hartwig, S.A. Maloy, S. J. Zinkle, T.R. Allen, H. Wang, X. Zhang, Superior radiation-resistant nanoengineered austenitic 304L stainless steel for applications in extreme radiation environments, Sci. Rep. 5 (2015) 7801, https://doi.org/10.1038/srep07801.
[6] L. Kurpaska, I. Jozwik, M. Lewandowska, J. Jagielski, The effect of Ar-ion irradiation on nanomechanical and structural properties of ODS RAF steels manufactured by using HIP technique, Vacuum 145 (2017) 144–152, https://doi.org/10.1016/j.vacuum.2017.08.039.
[7] A.R. Kilmametov, D.V. Gunderov, R.Z. Valiev, A.G. Balogh, H. Hahn, Enhanced ion irradiation resistance of bulk nanocrystalline TiNi alloy, Scripta Mater. 59 (2008) 1027–1030, https://doi.org/10.1016/j.scriptamat.2008.06.051.
[8] W. Mohamed, B. Miller, D. Porter, K. Murty, The role of grain size on neutron irradiation response of nanocrystalline copper, Materials 9 (2016) 144, https://doi.org/10.3390/ma9030144.
[9] A. Kozlovskiy, D. Shlimas, M. Zdorovets, Investigation of the effect of ionizing radiation on the structural and conductive characteristics of Ni nanostructures, Vacuum 163 (2019) 103–109, https://doi.org/10.1016/j.vacuum.2019.02.015.
[10] X.M. Bai, A.F. Voter, R.G. Hoagland, M. Nastasi, B.P. Uberuaga, Efficient annealing of radiation damage near grain boundaries via interstitial emission, Science 327 (2010) 1631–1634, https://doi.org/10.1126/science.1183723.
[11] X. Li, W. Liu, Y. Xu, C.S. Liu, B.C. Pan, Y. Liang, Q.F. Fang, J.-L. Chen, G.N. Luo, G.-H. Lu, Z. Wang, Radiation resistance of nano-crystalline iron: coupling of the fundamental segregation process and the annihilation of interstitials and vacancies near the grain boundaries, Acta Mater. 109 (2016) 115–127, https://doi.org/10.1016/j.actamat.2016.02.028.
[12] N. van Dijk, S. van der Zwaag, Self-healing phenomena in metals, Adv. Mater. Interfaces 5 (2018), 1800226, https://doi.org/10.1002/admi.201800226.
[13] J. Li, K.Y. Yu, Y. Chen, M. Song, H. Wang, M.A. Kirk, M. Li, X. Zhang, In situ study of defect migration kinetics and self-healing of twin boundaries in heavy ion irradiated nanotwinned metals, Nano Lett. 15 (2015) 2922–2927, https://doi.org/10.1021/nl504677z.
[14] Y. Chen, K.Y. Yu, Y. Liu, S. Shao, H. Wang, M.A. Kirk, J. Wang, X. Zhang, Damage-tolerant nanotwinned metals with nanovoids under radiation environments, Nat. Commun. 6 (2015) 7036, https://doi.org/10.1038/ncomms8036.
[15] M.A. Meyers, U.R. Andrade, A.H. Chokshi, The effect of grain size on the high-strain, high-strain-rate behavior of copper, Metall. Mater. Trans. 26 (1995) 2881–2893, https://doi.org/10.1007/BF02669646.
[16] J.L. Sun, P.W. Trimby, X. Si, X.Z. Liao, N.R. Tao, J.T. Wang, Nano twins in ultrafine-grained Ti processed by dynamic plastic deformation, Scripta Mater. 68 (2013) 475–478, https://doi.org/10.1016/j.scriptamat.2012.11.025.
[17] C. Dai, P. Saidi, Z. Yao, L.K. Béland, M.R. Daymond, Deformation-free nanotwin formation in zirconium and titanium, Mater. Lett. 247 (2019) 111–114, https://doi.org/10.1016/j.matlet.2019.03.029.
[18] A.D. Marwick, On the simulation of CTR neutron radiation damage by heavy ion irradiation, J. Nucl. Mater. 56 (1975) 355–358, https://doi.org/10.1016/0022-3115(75)90054-9.
[19] Y. Fu, G. Wang, J. Gao, Q. Yao, W.Tong, new approach to produce a nanocrystalline layer on surface of a large size pure titanium plate, Coatings 10 (2020) 430, https://doi.org/10.3390/coatings10050430.
[20] H. Wang, Ch Ban, N. Zhao, Y. Kang, T. Qin, S. Liu, J. Cui, Enhanced strength and ductility of nano-grained titanium processed by two-step severe plastic deformation, Mater. Lett. 266 (2020), 127485, https://doi.org/10.1016/j.matlet.2020.127485.
[21] S. Chen, Q. Sun, L. Qiao, J. Sun, Thermal stability of microstructure and mechanical properties of ultrafine-grained pure titanium. Proceedings of 13th International Conference on Fracture (2013).
[22] Z. Li, L. Fu, B. Fu, A. Shan, Effects of annealing on microstructure and mechanical properties of nano-grained titanium produced by combination of asymmetric and symmetric rolling, Mater. Sci. Eng. A 558 (2012) 309–318, https://doi.org/10.1016/j.msea.2012.08.005.
[23] P. Budzynski, V.A. Skuratov, T. Kochanski, Z. Surowiec, Titanium surface layers after irradiation with swift Kr and Xe ions, Vacuum 83 (2009) S190–S192, https://doi.org/10.1016/j.vacuum.2009.01.060.
[24] P. Horodek, J. Dryzek, Positron lifetime studies of defects distribution in Xe^{26+} irradiated pure titanium, Surf. Coating. Technol. 355 (2018) 247–251, https://doi.org/10.1016/j.surfcoat.2018.01.084.
[25] B.S. Rodchenkov, A.V. Kozlov, Yu G. Kuznetsov, G.M. Kalinin, Yu S. Strebkov, Irradiation behavior of titanium alloys for ITER blanket modules flexible attachment, J. Nucl. Mater. 307–311 (2002) 421–425, https://doi.org/10.1016/S0022-3115(02)01011-5.
[26] M. Griffiths, D. Faulkner, R.C. Styles, Neutron damage in α-titanium, J. Nucl. Mater. 119 (1983) 189–207, https://doi.org/10.1016/0022-3115(83)90196-4.
[27] X.S. Guan, Z.F. Dong, D.Y. Li, Surface nanocrystallization by sandblasting and annealing for improved mechanical and tribological properties, Nanotechnology 16 (2005) 2963–2971, https://doi.org/10.1088/0957-4484/16/12/040.
[28] X.P. Jiang, X.Y. Wang, J.X. Li, D.Y. Li, C.-S. Man, M.J. Shepard, T. Zhai, Enhancement of fatigue and corrosion properties of pure Ti by sandblasting, Mater. Sci. Eng. A 429 (2006) 30–35, https://doi.org/10.1016/j.msea.2006.04.024.
[29] J. Dryzek, K. Siemek, Defects and their range in pure bismuth irradiated with swift Xe ions studied by positron annihilation techniques, Appl. Phys. A 125 (2019) 85, https://doi.org/10.1007/s00339-018-2367-x.
[30] K. Siemek, M. Kulik, M. Eseev, M. Wróbel, A. Kobets, O. Orlov, A. Sidorin, Surface and subsurface defects studies of dental alloys exposed to sandblasting, Acta

Metall. Sin.-Engl. 32 (2019) 1181–1194, https://doi.org/10.1007/s40195-019-00884-5.
[31] E. Stepanova, Y. Bordulev, V. Kudiiarov, R. Laptev, A. Lider, J. Xinming, Effect of hydrogen on the structural and phase state and defect structure of titanium alloy, AIP Conf. Proc. 1772 (2016), 030016, https://doi.org/10.1063/1.4964554.
[32] J. Čížek, O. Melikhova, Z. Barnovská, I. Procházka, R.K. Islamgaliev, Vacancy clusters in ultrafine grained metals prepared by severe plastic deformation, J. Phys. Conf. Ser. 443 (2013), 012008, https://doi.org/10.1088/1742-6596/443/1/012008.
[33] D. Connétable, J. Huez, E. Andrieu, C. Mijoule, First-principles study of diffusion and interactions of vacancies and hydrogen in hcp-titanium, J. Phys. Condens. Matter 23 (2011), 405401, https://doi.org/10.1088/0953-8984/23/40/405401.
[34] J. Dryzek, A. Czapla, E. Kusior, Positron annihilation studies of the multilayer Cu-Cu_3Sn system, J. Phys. Condens. Matter 10 (1998) 10827–10838, https://doi.org/10.1088/0953-8984/10/48/006.
[35] K. Haynes, X. Hu, B.D. Wirth, Ch Hatem, K.S. Jones, Ultralow energy, elevated temperature implants of high doses of helium into silicon, in: Proceedings 22nd International Conference on Ion Implantation Technology 2018, IEEE, Würzburg, Germany, 2019, pp. 125–127, https://doi.org/10.1109/IIT.2018.8807968.
[36] P. Horodek, A.G. Kobets, I.N. Meshkov, A.A. Sidorin, O.S. Orlov, Slow positron beam at the JINR, Dubna, Nukleonika 60 (2015) 725–728, https://doi.org/10.1515/nuka-2015-0130.
[37] J. Kansy, Microcomputer program for analysis of positron annihilation lifetime spectra, Nucl. Instrum. Methods Phys. Res. 374 (1996) 235–244, https://doi.org/10.1016/0168-9002(96)00075-7.
[38] J. Dryzek, D. Singleton, Implantation profile and linear absorption coefficients for positrons injected in solids from radioactive sources ^{22}Na and ^{68}Ge\$^{68}$Ga, Nucl. Instrum. Methods Phys. Res. B 252 (2006) 197–204, https://doi.org/10.1016/j.nimb.2006.08.017.
[39] S.J. Zinkle, J.T. Busby, Structural materials for fission & fusion energy, Mater. Today 12 (2009) 12–19, https://doi.org/10.1016/S1369-7021(09)70294-9.
[40] J.M. Campillo Robles, F. Plazaola, Collection of data on positron lifetimes and vacancy formation energies of the elements of the periodic table, Defects and Diffusion Forum, Trans Tech Publications Ltd. 141 (2003) 213–215. www.scientific.net/DDF.213-215.141.
[41] J.M. Campillo Robles, E. Ogando, F. Plazaola, Positron lifetime calculation for the elements of the periodic table, J. Phys. Condens. Matter 19 (2007), 176222, https://doi.org/10.1088/0953-8984/19/17/176222.
[42] J. Dryzek, K. Siemek, The multi-scattering model for calculations of positron spatial distribution in the multilayer stacks, useful for conventional positron measurements, J. Appl. Phys. 114 (2013), 074904, https://doi.org/10.1063/1.4818578.
[43] B. Oberdorfer, R. Würschum, Positron trapping model for point defects and grain boundaries in polycrystalline materials, Phys. Rev. B 79 (2009) 184103, https://doi.org/10.1103/PhysRevB.79.184103.
[44] Q. Yao, G. Zhang, Y. Gao, W. Tong, The effect of mechanical shot blasting in producing the surface ultrafined grain layer on large-size titanium plate, in: Han Y (Ed.), Proceedings of Chinese Materials Conference 2017, Springer, Singapore, 2018, pp. 127–134, https://doi.org/10.1007/978-981-13-0107-0_12.
[45] P. Scherrer, Bestimmung der Grösse und der inneren Struktur von Kolloidteilchen mittels Röntgenstrahlen, Nachr. Ges. Wiss. Göttingen 26 (1918) 98.
[46] J.F. Ziegler, SRIM-2003. Nucl. Instrum. Methods phys, Res. B 219–220 (2004) 1027, https://doi.org/10.1016/j.nimb.2004.01.208.
[47] J. Dryzek, P. Horodek, GEANT4 simulation of slow positron beam implantation profiles, Nucl. Instrum. Methods Phys. Res. B 266 (2008) 4000–4009, https://doi.org/10.1016/j.nimb.2008.06.033.
[48] A. Van Veen, H. Schut, M. Clement, A. Kruseman, M.R. Ijpma, J.M.M. De Nijs, VEPFIT applied to depth profiling problems, Appl. Surf. Sci. 85 (1995) 216–224, https://doi.org/10.1016/0169-4332(94)00334-3.
[49] K.A. Iskhakov, I.V. Istomin, Study of point-defect-impurity atom (He,Xe) complexes by channeling method, USSR FEI–1755 18 (17) (1985), 18070928. https://inis.iaea.org/search/search.aspx?orig_q=RN:18070928.
[50] A.T. Raji, R. Mazzarello, S. Scandolo, S. Nsengiyumva, M. Harting, D.T. Britton, Intrinsic defects and krypton impurity atoms in hcp titanium: a first principles study, Phys. Rev. B 83 (2011), 054120, https://doi.org/10.1103/PhysRevB.83.054120.
[51] G. Dobmann, S.N. Korshunov, M. Kroening, YuV. Martynenko, I.D. Skorlupkin, A. S. Surkov, Helium and radiation defect accumulation in metals under stress, Vacuum 82 (2008) 856–866, https://doi.org/10.1016/j.vacuum.2008.01.044.
[52] H.A. Vasco, T.T. Hlatshwayo, S.V. Motloung, M. Mlambo, B.S. Mwankemwa, S. Petrovic, V.A. Skuratov, Effect of swift heavy ion irradiation in the migration behavior of Xe implanted into TiN, Vacuum 163 (2019) 59–68, https://doi.org/10.1016/j.vacuum.2019.01.054.